Analysis of membrane distillation crystallization system for high salinity brine treatment with zero discharge using Aspen flowsheet simulation

Wang, Rong; Wicaksana, Filicia; Yang, Xing; Fane, Anthony Gordon; Guan, Guoqiang

2012

Guan, G., Wang, R., Wicaksana, F., Yang, X., & Fane, A. G. (2012). Analysis of membrane distillation crystallization system for high salinity brine treatment with zero discharge using Aspen flowsheet simulation. Industrial & engineering chemistry research, 51(41), 13405-13413.

https://hdl.handle.net/10356/100769

https://doi.org/10.1021/ie3002183

Analysis of membrane distillation crystallization system for high salinity brine treatment with zero discharge using Aspen flowsheet simulation

Guoqiang Guan[a,b,c], *Rong Wang*[b,c,*], *Filicia Wicaksana*[b,c], *Xing Yang*[b,c], *Anthony G. Fane*[b,c]

[a] School of Chemistry and Chemical Engineering, Southern China University of Technology, Guangzhou, 510640, P. R. China

[b] School of Civil and Environmental Engineering, Nanyang Technological University, 639798, Singapore;

[c] Singapore Membrane Technology Centre, Nanyang Technological University, 639798, Singapore;

KEYWORDS: membrane distillation crystallization; process simulation; energy consumption; high salinity, crystal blockage

ABSTRACT: An environmentally friendly membrane distillation crystallization (MDC) system is proposed to treat high salinity reverse osmosis (RO) brine with zero discharge. The raw brine from RO desalination plants is concentrated in direct contact MD to produce pure water and the concentrate is then crystallized to produce solid salts without secondary disposal. A comprehensive analysis on the MDC system has been performed by Aspen flowsheet simulation with a user customized MD model, which was verified by our previous experiments. Simulation results reveal that the total energy consumption is negligibly changed by integration of a crystallization unit into the system, as over 97.8 % of the energy was consumed by the heater of the MD sub-system. Higher inlet temperatures of both the feed and permeate streams in the MD module can improve the thermal efficiency. The introduction of a heat recovery unit in the MDC system, to recover the heat in the permeate for feed preheating, can increase the gain output ratio (GOR) by 28 %. Moreover, it is shown that in a hollow fiber MD module, the permeate yield is a linear function of the length-to-radius ratio of the membrane module, and a longer MD module can reduce the specific energy consumption. A relatively high feed flow rate is preferred to avoid the potential problem of crystal blockage in the MD module.

1. Introduction

Over the past decades, a tremendous growth in human population and industrial activities has resulted in a significant demand for fresh and clean water. Desalination of seawater is a widespread approach used to meet this demand, and reverse osmosis (RO) is recognized as one of the key technologies, evidenced by the fact that RO accounted for 53 % of global desalination production capacity by 2008 [1, 2]. However, RO has its limits. The brine stream from seawater desalination RO plant is typically 50 % of the feed stream and double the concentration (~70 g/L salts) with an osmotic pressure of about 50 bar. Further recovery of water by RO becomes more difficult due to the need for increasingly high pressures. The discharge of the brine concentrate to the ocean also imposes environmental challenges [3-5].

Membrane distillation (MD) is a thermally driven process, which can be used to remove water from aqueous solutions of inorganic solutes. The operation is realized by utilizing a micro-porous hydrophobic membrane which acts as a physical barrier separating a warm aqueous feed solution from a cool permeate, and through which only water vapor molecules are transported. The vapor pressure difference across the membrane serves as the driving force for the vapor transportation, which is not significantly affected by the feed concentration [6]. An additional advantage of MD systems can be achieved by using either low-grade heat such as waste heat in power plants, or solar or geothermal energy. A solar-powered MD process provides an attractive green solution to obtain fresh water [7-10].

Nevertheless, to date only a few studies have reported treatment of highly concentrated streams using MD technology [11-13]. In these applications, MD was used to concentrate a solution by solvent removal in vapor phase. Significant progress has been achieved when the MD concept is used as a novel technique for crystallization, particularly for the preparation of enzyme crystals [13]. Applications of the MD process have also been extended to waste water treatment [14] and fruit juice concentration [15]. An integration of MD with a crystallization unit could become a potential solution to treat high salinity brine without secondary disposal. This integration is referred to as Membrane Distillation Crystallization (MDC) and was introduced by Drioli and coworkers [12]. In the MDC system, raw brine is first concentrated using MD to produce pure water as the permeate; the concentrated brine is then crystallized in a crystallizer so that the entire raw brine will be converted to fresh water and salt crystals as products. There are several challenges to be overcome in order to develop a viable MDC process for concentrate brine treatment, which include unacceptable energy usage and potential crystallization in the module. Selecting proper operating conditions are crucial to prevent crystal deposition inside the membrane module [12, 16].

Energy consumption is a critical performance indicator of the MDC process. Most literature claims that high energy efficiency could be achieved by incorporating MD with crystallization but the specific energy consumption of the MDC system has not been provided. Therefore, the current study aims to design a MDC system and analyze the system performance for RO brine treatment with the aid of process simulation. Process simulation is one of the most powerful tools in modern industrial engineering and has been used by several researchers to successfully predict and optimize the performance of the MD system [17-20]. The focus of this work is on energy

consumption in the MDC system and the strategies to avoid module blockage due to local NaCl crystal formation.

2. Theory

2.1 Configuration of MDC system

In this simulation study, a direct contact membrane distillation (DCMD) unit, which is the most studied MD configuration [21, 22], is used to integrate with a cooling crystallization unit. The assumed MD module comprises 103 polyvinylidenefluoride (PVDF) hollow fiber membranes, which have an inner diameter of 0.98 mm and a wall thickness of 0.24 mm. The membranes are housed in a polypropylene (PP) tube with an inner diameter of 0.023 m and a length of 0.36 m. This MD module design is similar to that reported in our previous experimental MD work [23]. A cooling crystallizer with an internal stirrer and a cooling jacket was assumed to operate in the temperature range of 30-50 °C by a circulating water cooling sub-system. The simulation is based on the MDC process diagram shown in Figure 1. The raw brine, which is simplified as the aqueous sodium chloride (NaCl) solution with a mass fraction of 0.07 since NaCl is the main component in the RO brine discharge and RO is typically operated with 50% recovery from 0.035 NaCl seawater, is introduced into the feed tank and combined with the residual mother liquor. The mixed feed is first preheated through a heat exchanger and then introduced into the MD module. In order to mitigate the temperature and concentration polarization phenomena [24], both the feed and permeate streams of MD module are re-circulated during the process. The permeate produced by the MD module over-flows into the permeate tank and the concentrated brine with NaCl mass fraction of 0.27 at over 60 °C is fed into the crystallizer, the temperature of

which is cooled down to 30 °C to facilitate the formation of salt crystals. Upon separation of salt crystals, the residual mother liquor is recycled into the system by mixing it with the raw brine stream.

2.2 Model development for MD module

The MD module is a key unit in the MDC system. In this section, a model is developed to simulate the heat and mass transfer in the MD module, which is then used as a customized unit for Aspen flowsheet simulation. In a well designed MD module, each section of hollow fiber should function in a similar manner, so the heat and mass transfer in each hollow fiber can be assumed to be the same. Hence, the following assumptions were made for simplicity: (1) the total amount of mass transfer in the MD module is equal to the number of hollow fiber membrane multiplied by the permeated mass of a single hollow fiber membrane; (2) the radial distributions of temperature and concentration in the MD module are homogeneous.

In a hollow fiber membrane as shown in Figure 2(a), the hot brine is assumed to be fed into the lumen and the cold water stream passes counter-currently outside the membrane (in the shell side). The hollow fiber membrane is axially divided into N elements, and a local-averaged temperature is used to express the local temperature in the element, if N is large enough. So, the temperatures of the feed and permeate streams can be expressed as the discrete lumen-side and discrete shell-side temperatures of each element, respectively.

In each element, shown in Figure 2(b), the heat transfer through the membrane consists of the latent heat transfer accompanying vapor flux and heat conduction loss [25]. If the heat transfer flux, J_H, is expressed in the form of overall heat transfer coefficient, H, it gives

$$J_H = H(T_{W,F} - T_{W,P}) = J_M \Delta h_V + \frac{\kappa_m}{\delta}(T_{W,F} - T_{W,P}) \tag{1}$$

where $T_{W,F}$ and $T_{W,P}$ are the membrane surface temperatures in the feed and permeate sides, respectively. Δh_V is the latent heat, κ_m is the membrane thermal conductivity and δ is the membrane wall thickness. If the transmembrane temperature difference is below 15 K, the mass transfer flux, J_M, can be written as

$$J_M = C\frac{dP}{dT}(T_{W,F} - T_{W,P}) \tag{2}$$

where C is the membrane distillation coefficient [6], and the gradient of vapor pressure, dP/dT, is obtained via the Antoine equation [6]. Combining Eqs.(1) and (2), the H is given by;

$$H = C\frac{dP}{dT}\Delta h_V + \frac{\kappa_m}{\delta} \tag{3}$$

The temperature polarization coefficient [25] is used to indicate the differences between the bulk temperatures and the membrane surface temperatures. Since the heat transfer fluxes through the thermal boundary layers (hot-side and cold-side) and the membrane are identical, the temperature polarization coefficient, τ, can be expressed as

$$\tau = \frac{T_{W,F} - T_{W,P}}{T_F - T_P} = \frac{1}{1 + H\left(\frac{1}{h_F} + \frac{1}{h_P}\right)} \tag{4}$$

where T_F and T_P are the bulk temperatures of the feed and permeate streams, and h_F and h_P are the film heat transfer coefficients of the feed and permeate sides, respectively. The geometric shape of a hollow fiber MD module is analogous to a shell and tube heat exchanger and their

heat transfer characteristics are very similar, so the film heat transfer coefficients can be estimated by similar correlations. To correlate the film heat transfer coefficients in the lumen (tube) side [26] and shell side [27], Eqs.(5) and (6) are used:

$$Nu = 3.66 + \frac{0.19Gz^{0.8}}{1 + 0.117Gz^{0.467}}\left(\frac{\mu}{\mu_W}\right)^{0.14} \quad \text{(lumen side)} \tag{5}$$

$$Nu = 0.16Re^{0.6}Pr^{0.33}\left(\frac{\mu}{\mu_W}\right)^{0.14} \quad \text{(shell side)} \tag{6}$$

The pressure drops, ΔP, in the tube and shell sides of the MD module can also be correlated as

$$\Delta P = \frac{fG^2L}{g\rho r}\left(\frac{\mu}{\mu_w}\right)^{-0.14} + n\frac{2G^2}{g\rho} \quad \text{, where } \begin{cases} n = 0 & \text{(shell side)} \\ n = 1 & \text{(lumen side)} \end{cases} \tag{7}$$

where *Gz*, *Nu*, *Pr* and *Re* are Graetz number, Nusselt number, Prandtl number and Reynolds number, respectively. *L* is the length of the MD module, *r* is the equivalent radius (i.e., inner radius for the lumen side, and hydrodynamic radius for the shell side), and *g* is the acceleration due to gravity. *G* is the mass flux which is equal to the product of density and velocity, i.e., $G = \rho u$, and *f* is the friction coefficient, i.e., $f = 16/Re$, when $Re < 2100$ [26].

When the bulk temperatures of the initial element are given, the film heat transfer coefficients can be estimated by Eqs.(5) and (6), so the temperature difference of the membrane surface could be obtained by Eq.(4). Once the heat and mass transfer flux in the element is computed by Eqs.(1) and (2), the bulk temperatures in the next element could be solved as

$$(2\pi r_i N \Delta L)J_H = \begin{cases} W_F C_{p,F}[T_F^{(i)} - T_F^{(i+1)}] & \text{(lumen side)} \\ W_P C_{p,P}[T_P^{(i-1)} - T_P^{(i)}] & \text{(shell side)} \end{cases} \tag{8}$$

After the evolution of bulk temperatures in each element are calculated, the temperature profiles of the MD module can be obtained by the discrete temperatures of the elements. Thus, the outlet

temperatures of the feed and permeate streams can be calculated for the MD module. The averaged mass transfer flux of the MD module was the arithmetic mean mass transfer flux of each element.

2.3 Aspen flowsheet simulation

The flowsheet simulation shown in Fig.1 was developed using Aspen™ One V7.2 (supplied by Aspen Technology, Inc., US). Accurate physicochemical property correlations are prerequisite, so the Aspen built-in electrolyte model "ELEC-NRTL" was selected by verification with data from the literature [28]. The solubility of NaCl in the aqueous solution is correlated by the ELEC-NRTL model. When the crystallizing temperature is below the saturating temperature, the amount of precipitation is calculated by the Aspen build-in subroutines and the solid crystal of NaCl is produced. An Aspen user customized unit model was developed to simulate the MD module based on the model described in section 2.2, which was coded in FORTRAN language and compiled by Intel© Visual Fortran V10 (supplied by Intel Inc., US). All other units, e.g., heaters, pumps and crystallizer, were created by the Aspen built-in units. In this simulation study, different process parameters were set at a steady state condition and solved by a sequential modular method.

3. Results and discussion

3.1 MD Model verification

The simulated MD results, obtained from the model in section 2.2, were compared with our previous experiments [23] where detailed description of the experiments can be found. Comparisons of simulated and experimental results of the feed and permeate outlet temperatures and permeation fluxes are presented in Figure 3. It can be seen that the simulated results are very consistent with the experimental data. Thus, the verified MD model was used as a customized unit for Aspen flowsheet simulation. Various process parameters, such as circulation flow rates and inlet temperature, etc., were adjusted to investigate the performance of the MDC system, especially the energy consumption.

3.2 Integration of MD with crystallization

In a steady-state operation, raw brine can be completely used to produce fresh water and solid salts in the MDC system (Figure 1). Based on the material balance, the relationships between the products and the raw material are given as;

$$W_P = W_B(1 - X_B); \quad W_S = W_B X_B \tag{9}$$

where W and X are the mass flow rate and the mass fraction of NaCl, respectively, and the subscripts of B, P and S indicate the raw brine, the permeate product stream and the solid product stream.

There are three circulation streams in the MDC system: a feed stream, a permeate stream and a recycle mother liquor stream. Each of them can be adjusted to make the MDC system meet the production needs as expressed by Eq.(9). If raw brines with different concentrations need to be recovered in the MDC system, the flow rates of the feed and permeate streams have to be adjusted accordingly. The operation curves relating the flow rates of the feed and permeate streams are drawn in Figure 4 for raw brines with different concentrations, X_B. When X_B is increased, the water production is reduced if the treatment capacity of the raw brine is fixed, so the flow rates need to be decreased accordingly.

The recycle mother liquor stream connects the MD sub-system with the crystallization. The salt production can be expressed by Eq.(10) based on the material balance.

$$W_S = W_1(X_1 - X_2)/(1 - X_1) \tag{10}$$

where subscripts 1 and 2 indicate the inlet and outlet of the crystallization unit. The outlet concentration (X_2) can be treated as a constant value, because NaCl with a concentration of X_2 is saturated at the crystallizing temperature, which is constant in a crystallizer operated under a steady-state condition. In steady-state operation, W_S is constant so the inlet concentration (X_1) of the crystallizer increases with a decrease in W_1. A higher X_1 is favorable for crystallization. However, a high concentration of the feed stream in the MD increases the potential of crystal blockage in the MD sub-system, and this is discussed in the next section.

3.3 Potential of crystal blockage in MD module

The brine concentration in the MD feed is relatively high, and it could nearly reach its saturation level. Therefore, possible crystal blockage in the MD module is a practical concern in the MDC system [12]. The simulated temperature and concentration profiles along the hollow fiber membranes under different operating conditions are shown in Figure 5 along with NaCl saturation concentration at different temperatures, which can be used to evaluate the risk of MD module blockage and determine proper operating conditions to avoid the problem.

It can be seen that operation at a low feed flow rate causes a greater temperature gradient along the hollow fiber membranes. For example, the outlet temperature of the feed stream is found to be 74 °C at a high feed flow rate (W_{R1}=54.8 kg/h), but it is reduced significantly to 42 °C at a low feed flow rate operation (W_{R1}=3.4 kg/h). The low feed flow rate also causes a high feed concentration, as the removed water from the feed stream needs to meet the steady-state operation so that the same amount of water is required to be removed from the feed stream in either low or high feed flow rates.

The gap between the local NaCl mass fraction and the saturation mass fraction is an indicator for the potential of membrane blockage by the crystals. If the concentration in the feed side is always far below the saturation level along the entire length of the module, the tendency of blockage in the MD module is very low. Obviously, a high feed flow rate can help reduce the risk of NaCl being crystallized within the module.

3.4 Energy consumption distribution in the MDC system

The energy consumption in the MDC system is a critical index to evaluate the process performance. In the simulation all unit processes (pumps, heater, cooler and crystallizer) are assumed to operate as ideal cases so the required energy, which includes the thermal energy in the heater, electricity to drive the pumps, and mechanical energy to drive the Carnot refrigerated cycle to produce the required cooling duties for the cooler and crystallizer, would be at its lowest limit. Various process parameters, such as flow rates, inlet temperatures, etc., can affect the energy consumption. As reported in the literature [29], high feed and permeate flow rates have little effect on the permeate flux enhancement, but the permeation flux increases monotonically with the inlet temperature of the feed stream. This suggests that the inlet temperature has a significant influence on the specific energy consumption in the MDC system. Thus, energy consumption analysis was performed by varying the inlet temperatures of the feed and permeate streams.

Figure 6 shows that the energy consumption of the crystallization sub-system is less than 0.5 % of the total energy consumption of the MDC system. This suggests that the crystallization unit has negligible influence on the total energy consumption of the MDC system. Moreover, it is found that over 97.8 % of energy needed in the MDC system is consumed by the heater (Figure 7). It can be reduced if the inlet temperature of the feed is high and the inlet temperature of the permeate is low. The benefit from the higher feed temperature comes from a lower contribution to overall heat transfer by conductive heat loss through the membrane; this is discussed further in 3.5.2.

In the MD process, water removal is a three step process: evaporation at the feed-side surface of the membrane, vapor transport across the membrane followed by the condensation at the permeate-side surface of the membrane. The high heat energy requirement is mainly caused by the amount of heat energy input to evaporate the water, i.e., the latent heat, which is usually much larger than the energy needed for pumping fluid. A further discussion on various strategies to enhance energy utilization is provided in the next section.

3.5 Methods for enhancing energy utilization

As discussed in section 3.4, the heater accounts for the largest portion of energy consumption in the MDC system. The improvement of heat utilization can enhance energy efficiency. This can be achieved by optimizing the process parameters and adopting heat recovery techniques. In addition, the geometric parameters of the MD module can be optimized to increase the permeate flux, thereby reducing the specific energy consumption.

3.5.1 Effect of permeation yield in MD

In the MD process, a permeation yield, y, is defined as the ratio of the transmembrane mass flow rate (W_p) to the feed mass flow rate (W_{R1}). The permeation yield relates to the mass flux J_M and the geometric characteristics of the MD module as follows:

$$y = \frac{W_P}{W_{R1}} = \frac{2L}{r}\frac{J_M}{G} \tag{11}$$

Figure 8 shows the simulation result of permeation flux as a function of feed mass flux. A very linear relationship between simulated J_M/G and y with zero intercept can be observed. These

results are consistent with the above analysis and reconfirmed the validity of the simulation approach. The permeation yield can be used as a performance indicator of the membrane separation process. A higher permeation yield would result in a greater permeate product with the same amount of the feed so the specific energy consumption can be reduced.

A large-scale raw brine treatment usually needs multiple MD modules. As shown in Eq.(11) a large L/r ratio can increase the permeation yield. Therefore, MD elements connected in series would have better performance compared to the parallel configuration. However, if L/r ratio is too large, the pressure drop would increase, leading to higher power consumption for pumping. In addition, the average permeate flux would decrease with longer MD modules as driving forces diminish [25]. Hence, there will be a trade-off between energy efficiency and capital plus operating costs.

3.5.2 Effect of thermal efficiency

Most of the energy input in the MDC system is used to supply heat in the MD process. In reality, only a portion of the heat is used to produce the permeate. Thermal efficiency, η, is the ratio of vaporization heat required to produce the permeate to the total heat transfer [30]. As seen from Eq.(1), the heat transfer across the membrane consists of two parts: the effective heat of evaporation and heat loss due to conduction across the membrane. High thermal efficiency of the system means low heat loss that can improve the energy utilization. Thermal efficiency is a function of membrane temperature if the membrane distillation coefficient and thermal conductivity of the membrane are assumed to be constant, as shown in Eq.(12)

$$\eta = \frac{1}{1 + \frac{\kappa_m}{\delta C} \frac{1}{\left(\Delta h_V \frac{dP}{dT}\right)_{T_M}}} \tag{12}$$

where T_M is defined as the mean of the membrane wall temperatures in the feed and permeate sides. The relation between the thermal efficiency and membrane temperature can be seen in Figure 9, where the thermal efficiency increases with an increase in membrane temperature. It suggests that operating MD at a high temperature is preferable.

3.5.3 Effect of heat recovery and Gain output ratio (GOR)

Heat recovery is commonly used to increase the energy efficiency. In the MD process, the heat in the feed stream is transferred to the permeate side through the condensation of permeating vapor and thermal conduction. So a heat recovery unit is introduced to preheat the feed stream by the permeate stream, as shown in Figure 1.

Gain output ratio (GOR) is a parameter widely used to indicate the energy efficiency in evaporation process [25, 30]. There are two outputs in the MDC system, i.e., pure water and solid salts. The GOR calculation in the MDC system is similar to that in the MD system except that the overall energy input is the energy consumption of MD system supplemented by the energy consumption of the crystallization unit.

The GOR in the MDC system without a heat recovery unit is given in Figure 10. The GOR values at various inlet temperatures are in the range of 0.545-0.615. This means that 1.6-1.8 kg of dry saturated steam is required to produce 1 kg of water permeate. Because MD without heat

recovery process has the same thermal nature as a single-stage flash distillation, the energy efficiency of both systems is comparable. The thermal efficiency of a single-stage flash distillation is usually about 0.656 for the feed's temperature drop of 20 °C and vapor-to-liquid temperature difference of 10 °C [26], so the GOR values of 0.545-0.615 are reasonable.

Figure 10 also shows that increase in the inlet temperatures of both the feed and permeate streams results in an increase of the GOR value, but the effect of the feed inlet temperature is more significant than that of the permeate inlet temperature. Raised inlet temperatures of both streams can lead to relatively high temperatures on both membrane surfaces. As shown in Figure 8, a higher membrane temperature would increase the thermal efficiency, thus operating MD under elevated inlet temperatures is preferred.

The use of a heat recovery system could reduce the workloads of the heater and cooler, hence improving the overall energy efficiency. The GOR in the MDC with a heat recovery unit is presented in Figure 11. With a heat recovery unit, the GOR value increased to 0.575-0.785, which is about 28 % maximum increase in the GOR. Because the inlet conditions of the MD module with the heat recovery unit are the same as those without the heat recovery unit, it is anticipated that the MD module would have a similar performance and the GOR would follow a similar trend that higher GOR values would be obtained at higher inlet temperatures. Therefore, the installation of a heat recovery unit could reduce more than 20 % of the energy consumption, with an increase in the capital cost.

Significantly higher GOR values can be found in the literature for MD systems [25, 30]. In those cases, extremely long membranes (several meters of membrane length) or low feed-side flow rates (Reynolds number was about 60) were applied. These two conditions seem to be unsuitable for the MDC system, as they have the potential of causing crystal blockage as discussed in section 3.3. If waste heat is available, over 90 % of the energy consumed in the MDC system can be provided, and the main electrical energy would be consumed in the pumps. Another strategy may be to use multiple effect vacuum MD, but great care would be needed to avoid module blockage. Alternatively a two stage MD could be used with a higher GOR option taking brine from 0.07 to, say, 0.25 mass fraction and the MDC approach described here using that as feed. The trade off is that the two stage MD could involve greater capital expenditure.

4. Conclusions

A steady state MDC system has been simulated to treat high salinity brine with zero discharge. RO brine with NaCl mass fraction of 0.07 would be concentrated by a hollow fiber DCMD module, and the concentrated stream would then be introduced to a cooling crystallizer to produce salt crystals. A comprehensive analysis on the MDC system has been performed using Aspen flowsheet simulation with a verified user customized MD model to determine the distribution of energy consumption, optimize operating conditions to avoid the crystal blockage in MD module and propose several strategies to enhance energy utilization.

- The addition of a crystallization unit into the MD system has little effect on the total energy consumption of the system. The proportion of energy consumption of the crystallization sub-

system is less than 0.5 % of the MDC system. Over 97.8 % of the total energy consumption is spent in the heater.

- The GOR is used to evaluate the energy efficiency in the MDC system. In this study, the highest GOR is 0.615, which is comparable to the thermal efficiency of a single stage flash distillation system.

- As most of energy input is consumed in the form of heating, the enhancement of thermal efficiency and the use of a heat recovery system can improve the energy utilization. Membrane temperature is shown to have a positive effect on the thermal efficiency, so high inlet temperatures of the MD module are favorable to reduce the energy consumption. A heat recovery unit, that recovers the heat in the permeate for feed preheating, can increase the GOR value by 28% (maximum).

- In a hollow fiber DCMD module, it is shown that the permeate yield is a linear function of the length-to-radius ratio (L/r) of the membrane module. A large L/r ratio can increase the permeation yield and reduce the specific energy consumption in the MDC, implying that MD modules connected in series are preferable to the in parallel configuration.

- A low feed flow rate in the MD module increases the risk of module blockage by NaCl crystals due to the large temperature drop and increased salt concentration along the module. Thus a high feed flow rate is preferred to avoid the potential problem of crystal blockage in the MD module.

AUTHOR INFORMATION

Corresponding Author

To whom correspondence should be addressed. Tel. (65) 6790 5327; email: rwang@ntu.edu.sg

Funding Sources

Environment and Water Industry Program Office of Singapore Project #0901-IRIS-02-03

ACKNOWLEDGMENT

This research grant is supported by the Singapore National Research Foundation under its Environmental & Water Technologies Strategic Research Programme and administered by the Environment & Water Industry Programme Office (EWI) of the PUB (EWI RFP 0901-IRIS-02-03). We also acknowledge funding support from the Singapore Economic Development Board to the Singapore Membrane Technology Centre. Useful discussions with Dr. Hui Yu and Dr. Yinghong Lu from SMTC, and technical support by Jolly (Aspen Technology Inc. US) are also acknowledged.

NOMENCLATURE

C Membrane distillation coefficient, kg m^{-2} Pa^{-1} s^{-1}

C_P Heat capacity, J kg^{-1} K^{-1}

f Friction coefficient

g Gravity accelerator, m s^{-2}

G Mass flux, kg m^{-2} s^{-1}

Gz	Graetz number
h	Film heat transfer coefficient, W m^{-2} K^{-1}
H	Overall heat transfer coefficient, W m^{-2} K^{-1}
J_H	Heat transfer flux, W m^{-2}
J_M	Mass transfer flux, kg m^{-2} s^{-1}
L	Length of membrane, m
n	Option integer, used in Eq. (7)
N	Number of hollow fiber membranes
Nu	Nusselt number
P	Pressure, Pa
Pr	Prandtl number
r	Radius of hollow fiber membrane
Re	Reynolds number
T	Bulk temperature
T_W	Membrane surface temperature, K
u	Velocity of fluid, m s^{-1}
W	Mass flow rate, kg s^{-1}

X Mass fraction of NaCl

y Permeation yield

Δh_V Latent heat, J kg^{-1}

Greek letters

δ Thickness of membrane, m

η Thermal efficiency

κ Thermal conductivity, W m^{-1} K^{-1}

μ Viscosity, Pa s

ρ Density, kg m^{-3}

τ Temperature polarization coefficient

Subscripts

1 Inlet mother liquor stream of crystallization

2 Recycle mother liquor stream

B Raw brine

F Feed stream

P Permeate stream

m Membrane

R1	Feed-side circulation stream
R2	Permeate-side circulation stream
S	Solid salt
W	Membrane surface

REFERENCES

1. http://desaldata.com.

2. Mehdizadeh, H., Membrane desalination plants from an energy-exergy viewpoint. *Desalination* **2006,** 191, (1-3), 200-209.

3. Hajbi, F.; Hammi, H.; M'nif, A., Reuse of RO Desalination Plant Reject Brine. *Journal of Phase Equilibria and Diffusion* **2010,** 31, (4), 341-347.

4. Mohamed, A. M. O.; Maraqa, M.; Al Handhaly, J., Impact of land disposal of reject brine from desalination plants on soil and groundwater. *Desalination* **2005,** 182, (1-3), 411-433.

5. Muñoz, I.; Fernández-Alba, A. R., Reducing the environmental impacts of reverse osmosis desalination by using brackish groundwater resources. *Water Research* **2008,** 42, (3), 801-811.

6. Curcio, E.; Drioli, E., Membrane distillation and related operations - A review. *Separation and Purification Reviews* **2005,** 34, (1), 35-86.

7. Ding, Z. W.; Liu, L. Y.; El-Bourawi, M. S.; Ma, R. Y., Analysis of a solar-powered membrane distillation system. *Desalination* **2005,** 172, (1), 27-40.

8. Hogan, P. A.; Sudjito; Fane, A. G.; Morrison, G. L., DESALINATION BY SOLAR HEATED MEMBRANE DISTILLATION. *Desalination* **1991,** 81, (1-3), 81-90.

9. Koschikowski, J.; Wieghaus, M.; Rommel, M., Solar thermal-driven desalination plants based on membrane distillation. *Desalination* **2003,** 156, (1-3), 295-304.

10. Charcosset, C., A review of membrane processes and renewable energies for desalination. *Desalination* **2009,** 245, (1-3), 214-231.

11. Charcosset, C.; Kieffer, R.; Mangin, D.; Puel, F., Coupling between Membrane Processes and Crystallization Operations. *Industrial & Engineering Chemistry Research* **2010,** 49, (12), 5489-5495.

12. Curcio, E.; Criscuoli, A.; Drioli, E., Membrane Crystallizers. *Industrial & Engineering Chemistry Research* **2001,** 40, (12), 2679-2684.

13. Di Profio, G.; Perrone, G.; Curcio, E.; Cassetta, A.; Lamba, D.; Drioli, E., Preparation of Enzyme Crystals with Tunable Morphology in Membrane Crystallizers. *Industrial & Engineering Chemistry Research* **2005,** 44, (26), 10005-10012.

14. Regel-Rosocka, M., A review on methods of regeneration of spent pickling solutions from steel processing. *Journal of Hazardous Materials* **2010,** 177, (1-3), 57-69.

15. Jiao, B.; Cassano, A.; Drioli, E., Recent advances on membrane processes for the concentration of fruit juices: a review. *Journal of Food Engineering* **2004,** 63, (3), 303-324.

16. Chan, T. M.; Fane, A. G.; Matheickal, J. T.; Sheikholeslami, R., Membrane distillation crystallization of concentrated salts—flux and crystal formation. *Journal of Membrane Science* **2005,** 257, (1–2), 144-155.

17. Bui, V. A.; Vu, L. T. T.; Nguyen, M. H., Simulation and optimisation of direct contact membrane distillation for energy efficiency. *Desalination* **2010,** 259, (1-3), 29-37.

18. Chang, H. A.; Wang, G. B.; Chen, Y. H.; Li, C. C.; Chang, C. L., Modeling and optimization of a solar driven membrane distillation desalination system. *Renewable Energy* **2010,** 35, (12), 2714-2722.

19. Zuo, G.; Wang, R.; Field, R.; Fane, A. G., Energy efficiency evaluation and economic analyses of direct contact membrane distillation system using Aspen Plus. *Desalination* **2011,** In Press, Corrected Proof.

20. Yu, H.; Yang, X.; Wang, R.; Fane, A. G., Numerical simulation of heat and mass transfer in direct membrane distillation in a hollow fiber module with laminar flow. *Journal of Membrane Science* **2011,** 384, (1–2), 107-116.

21. Khayet, M., Membranes and theoretical modeling of membrane distillation: A review. *Advances in Colloid and Interface Science* **2011,** 164, (1-2), 56-88.

22. El-Bourawi, M. S.; Ding, Z.; Ma, R.; Khayet, M., A framework for better understanding membrane distillation separation process. *Journal of Membrane Science* **2006,** 285, (1-2), 4-29.

23. Yang, X.; Wang, R.; Shi, L.; Fane, A. G.; Debowski, M., Performance improvement of PVDF hollow fiber-based membrane distillation process. *Journal of Membrane Science* **2011,** 369, (1-2), 437-447.

24. Schofield, R. W.; Fane, A. G.; Fell, C. J. D., Heat and mass transfer in membrane distillation. *Journal of Membrane Science* **1987,** 33, (3), 299-313.

25. Fane, A. G.; Schofield, R. W.; Fell, C. J. D., The efficient use of energy in membrane distillation. *Desalination* **1987,** 64, 231-243.

26. Perry, R. H.; Green, D. W.; Maloney, J. O., *Perry's chemical engineers' handbook*. McGraw-Hill Companies, Inc.: New York, 1997.

27. Short, B. E., Flow geometry and heat exchanger performance. *Chemical Engineering Progress* **1965,** 61, (7), 63-70.

28. Sparrow, B. S., Empirical equations for the thermodynamic properties of aqueous sodium chloride. *Desalination* **2003,** 159, (2), 161-170.

29. Gryta, M., Concentration of NaCl solution by membrane distillation integrated with crystallization. *Separation Science and Technology* **2002,** 37, (15), 3535-3558.

30. Gilron, J.; Song, L.; Sirkar, K. K., Design for Cascade of Crossflow Direct Contact Membrane Distillation. *Industrial & Engineering Chemistry Research* **2007,** 46, (8), 2324-2334.

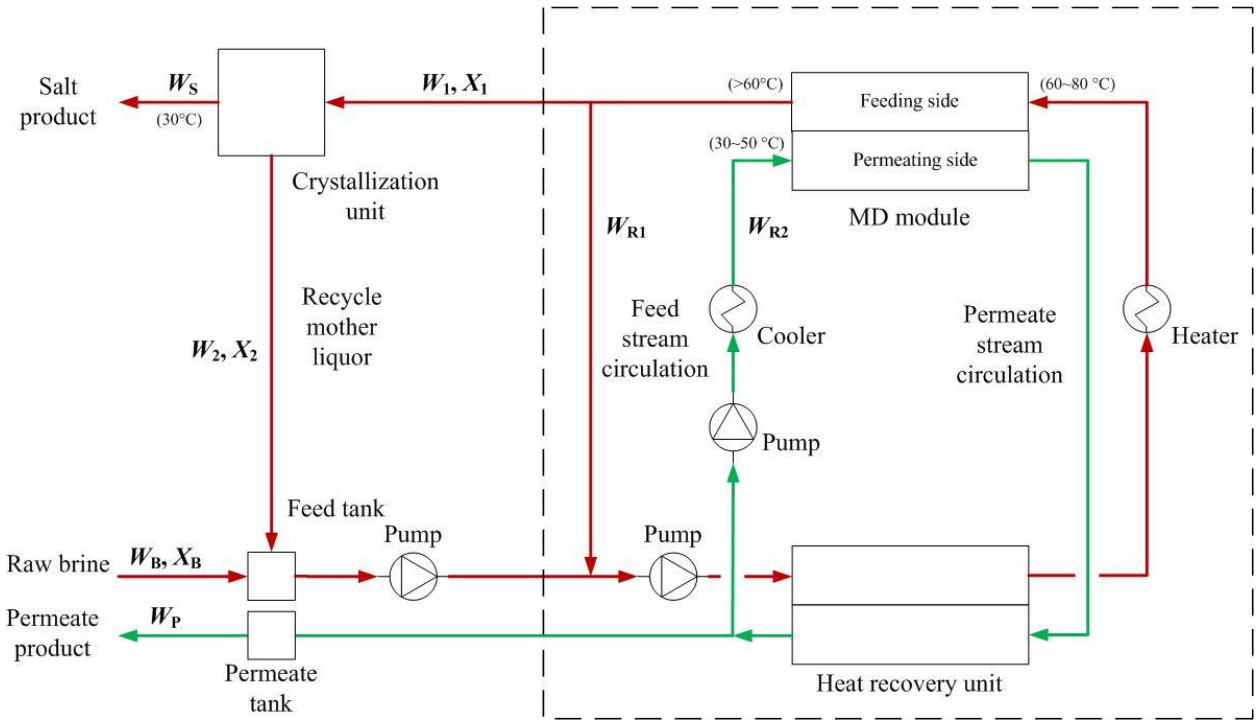

Figure 1: Diagram of membrane distillation crystallization process

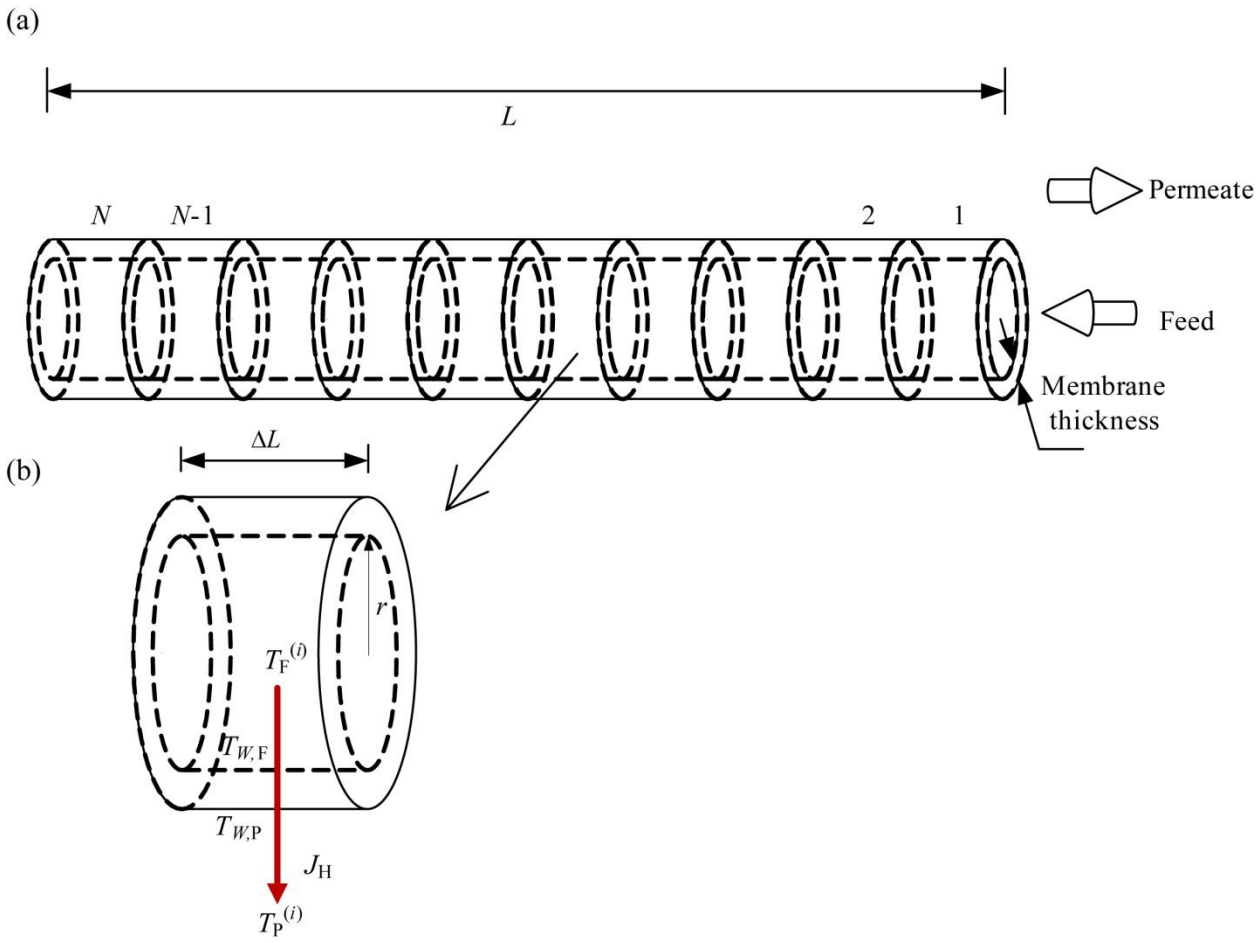

Figure 2: Model of membrane distillation process

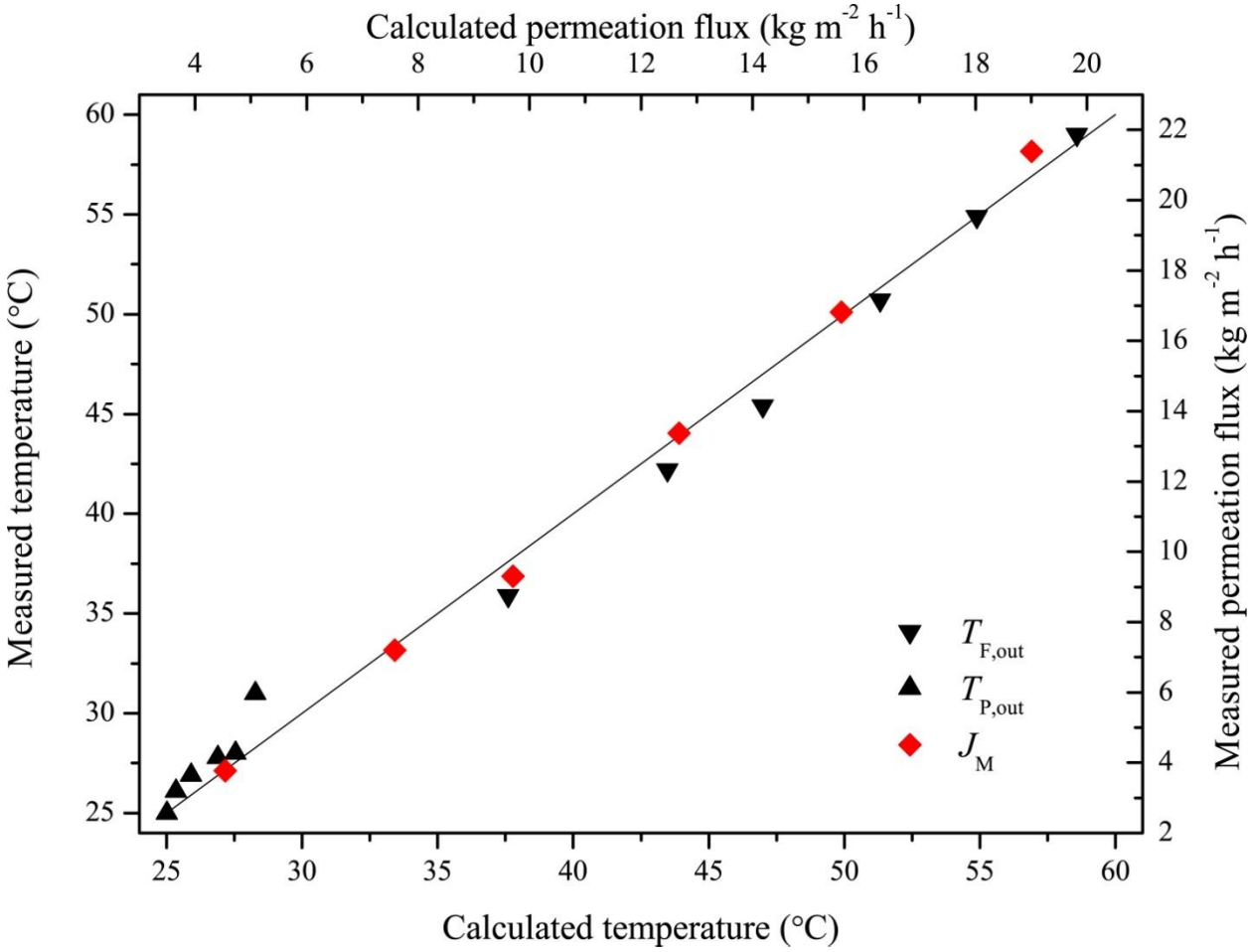

Figure 3: Comparison of outlet temperatures and permeation fluxes between simulated and experimental results of the MD module

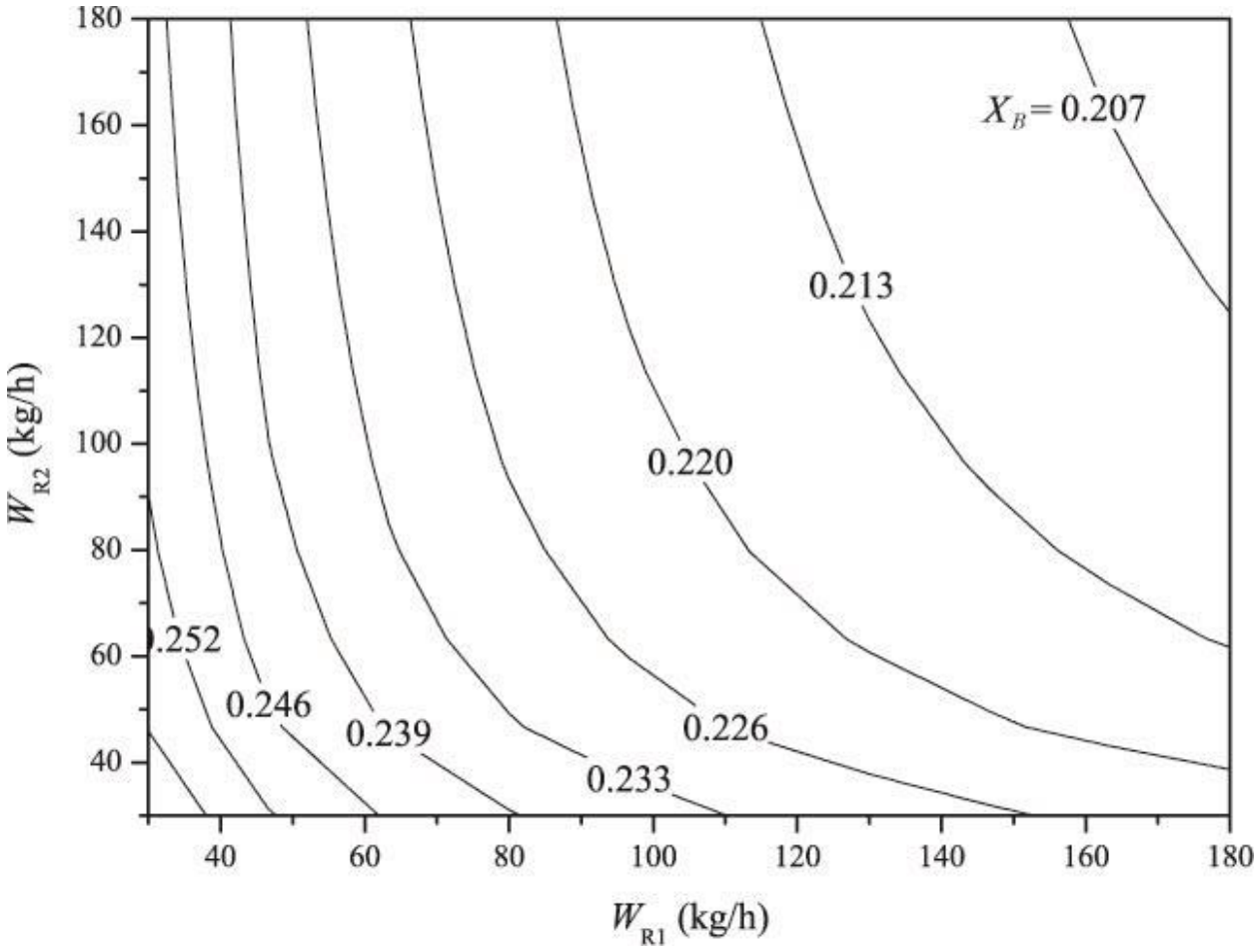

Figure 4: Operating curves of the feed and permeate streams at different NaCl mass fractions of raw brine

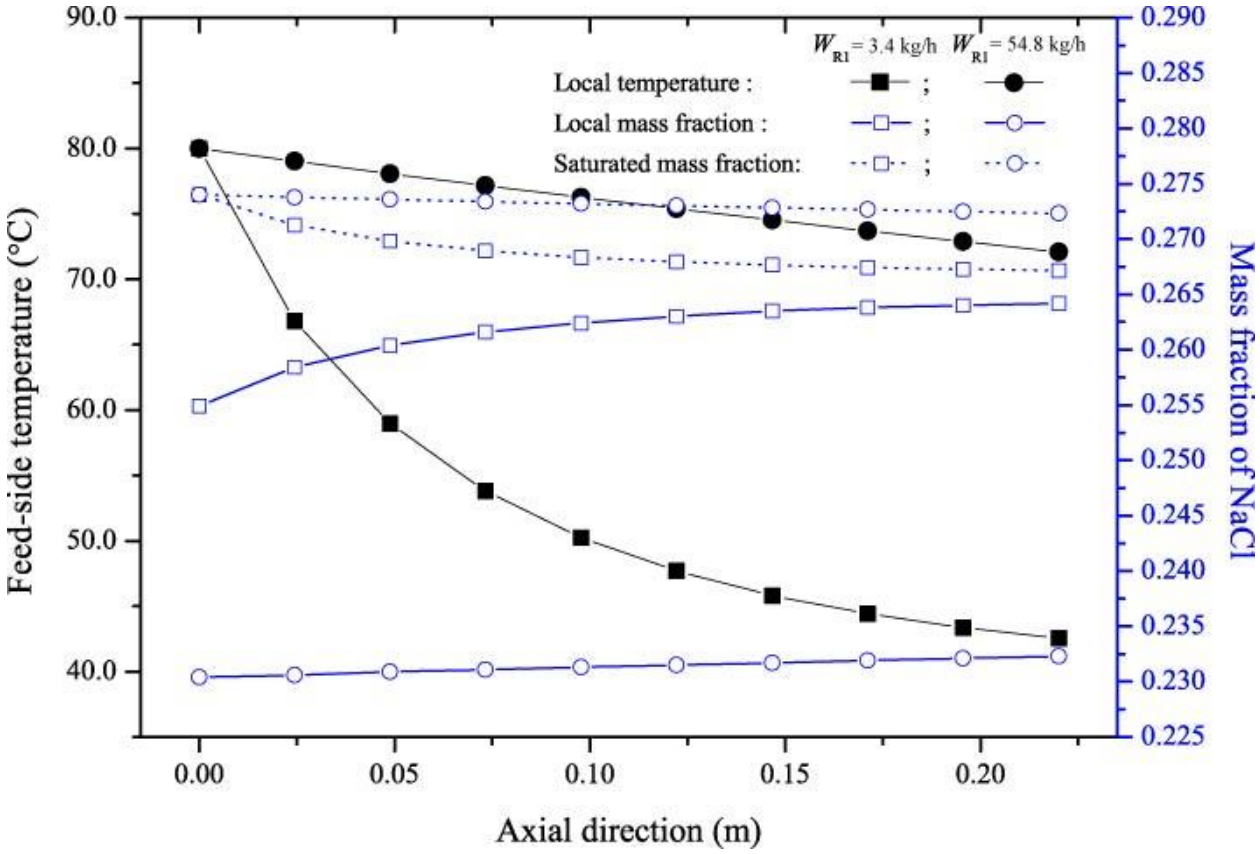

Figure 5: Profiles of temperature and concentration along the MD module

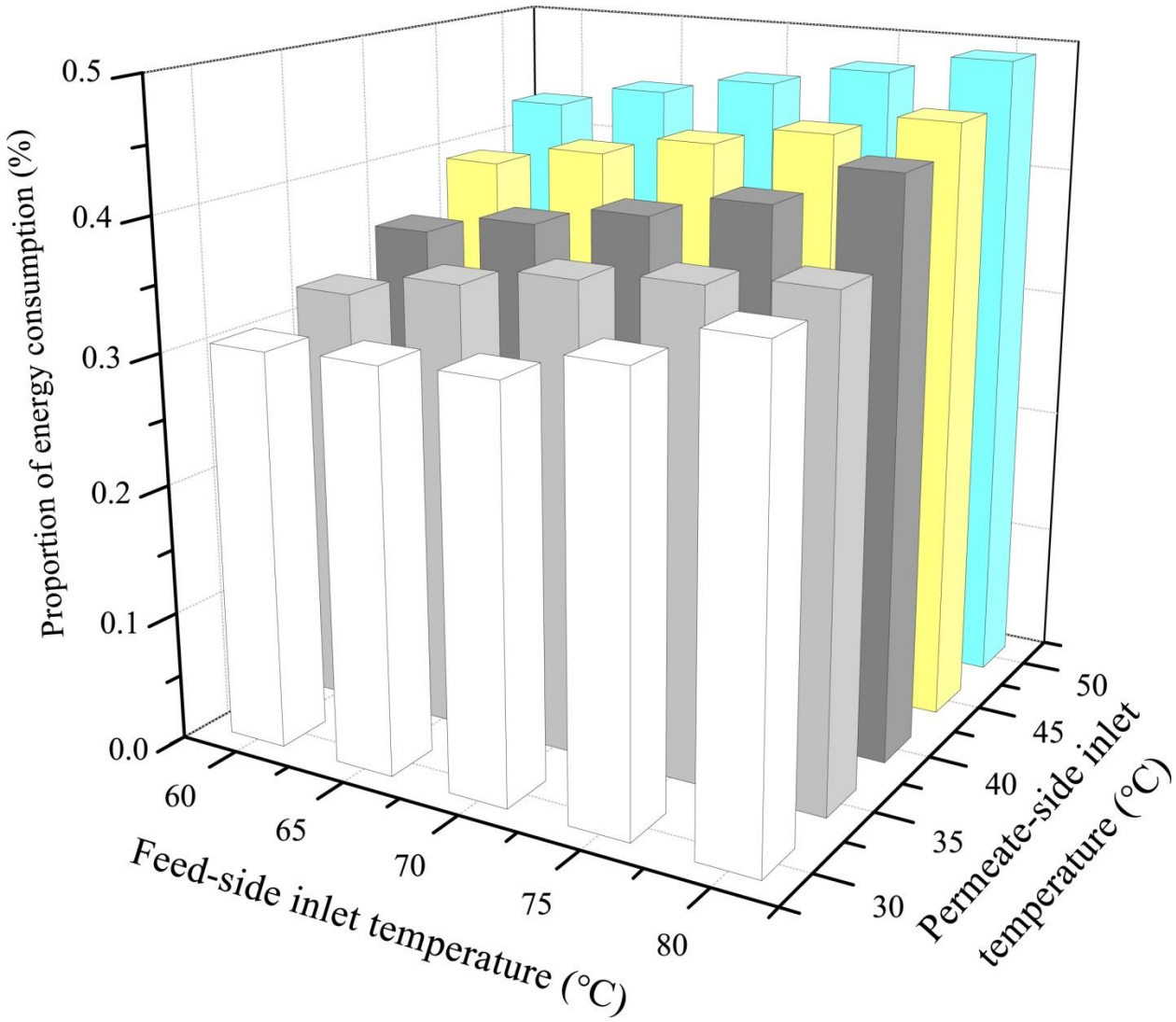

Figure 6: Proportion of energy consumption for crystallization in the MDC system

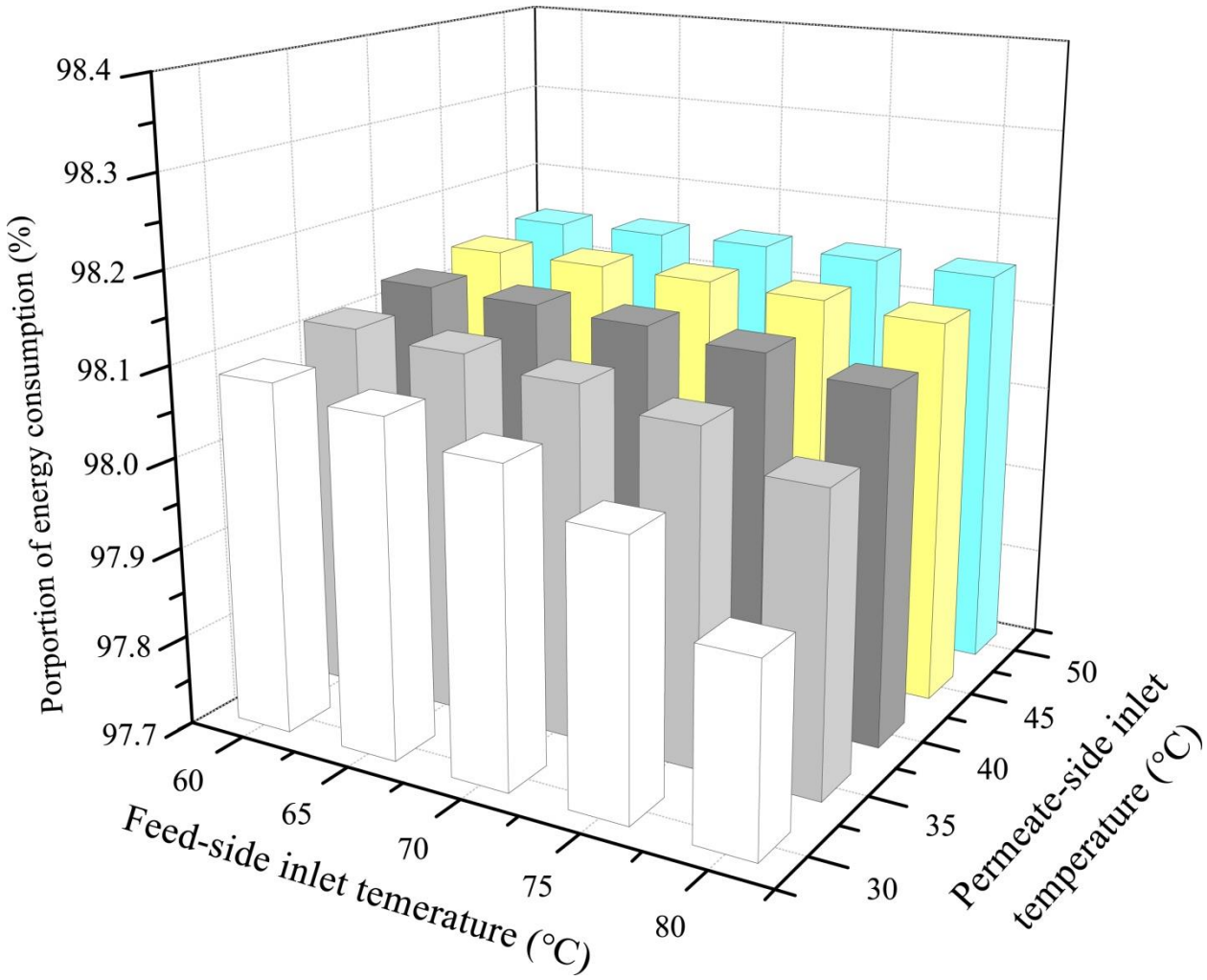

Figure 7: Proportion of energy consumption for the heater in the MDC system

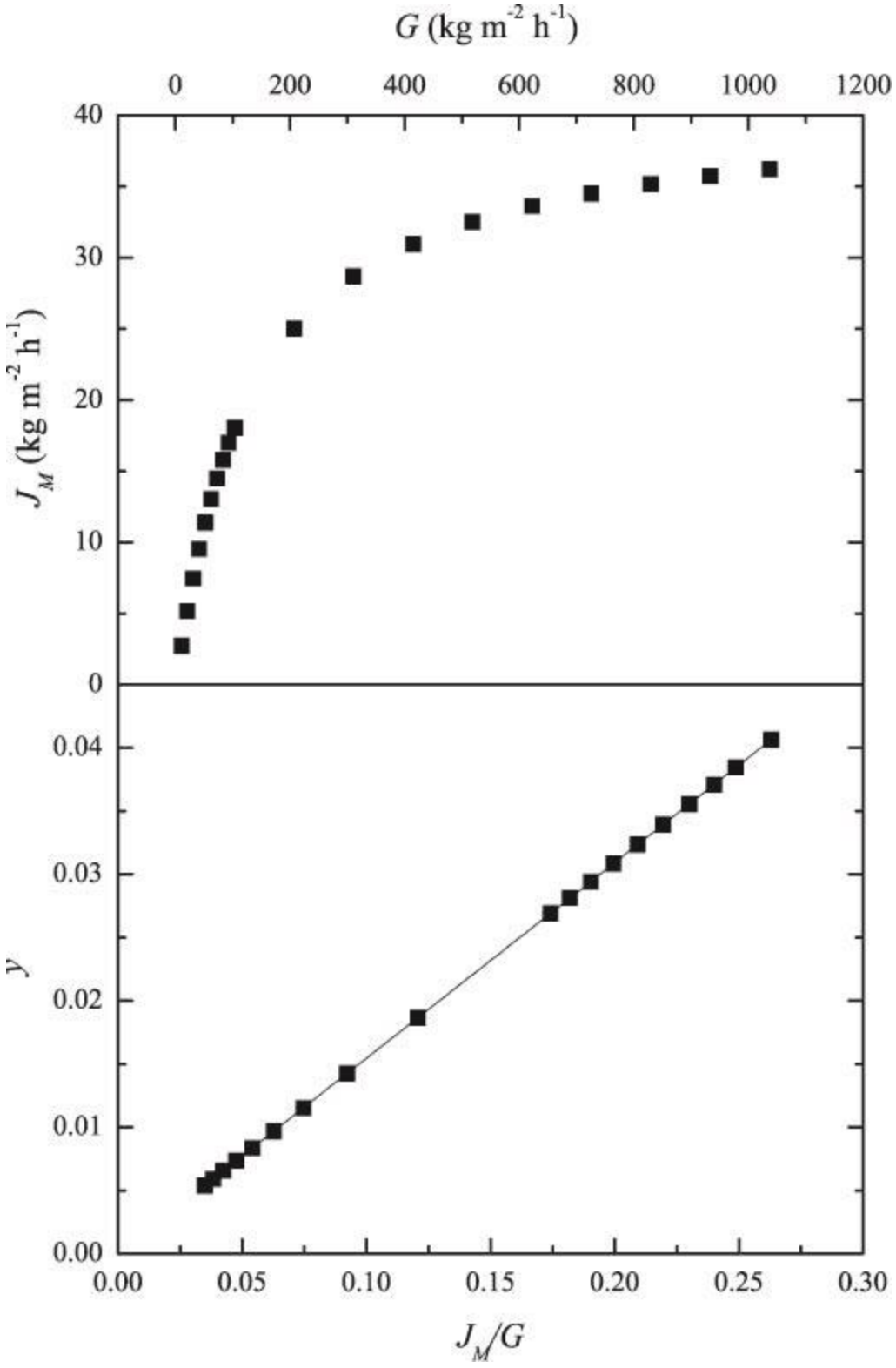

Figure 8: Permeation yield vs. the ratio of permeation flux to feed mass flux

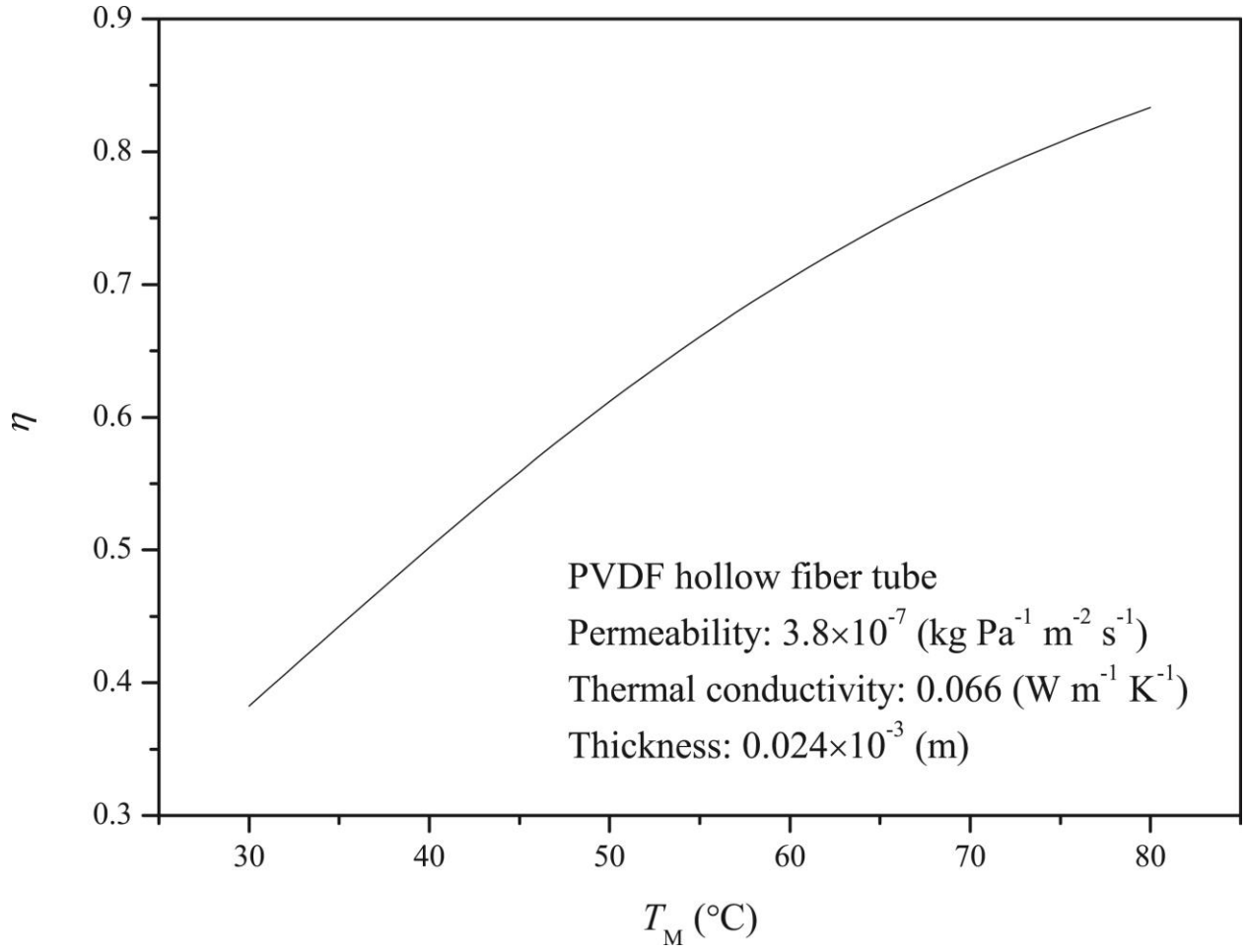

Figure 9: Thermal efficiency vs. membrane temperature in the MD module

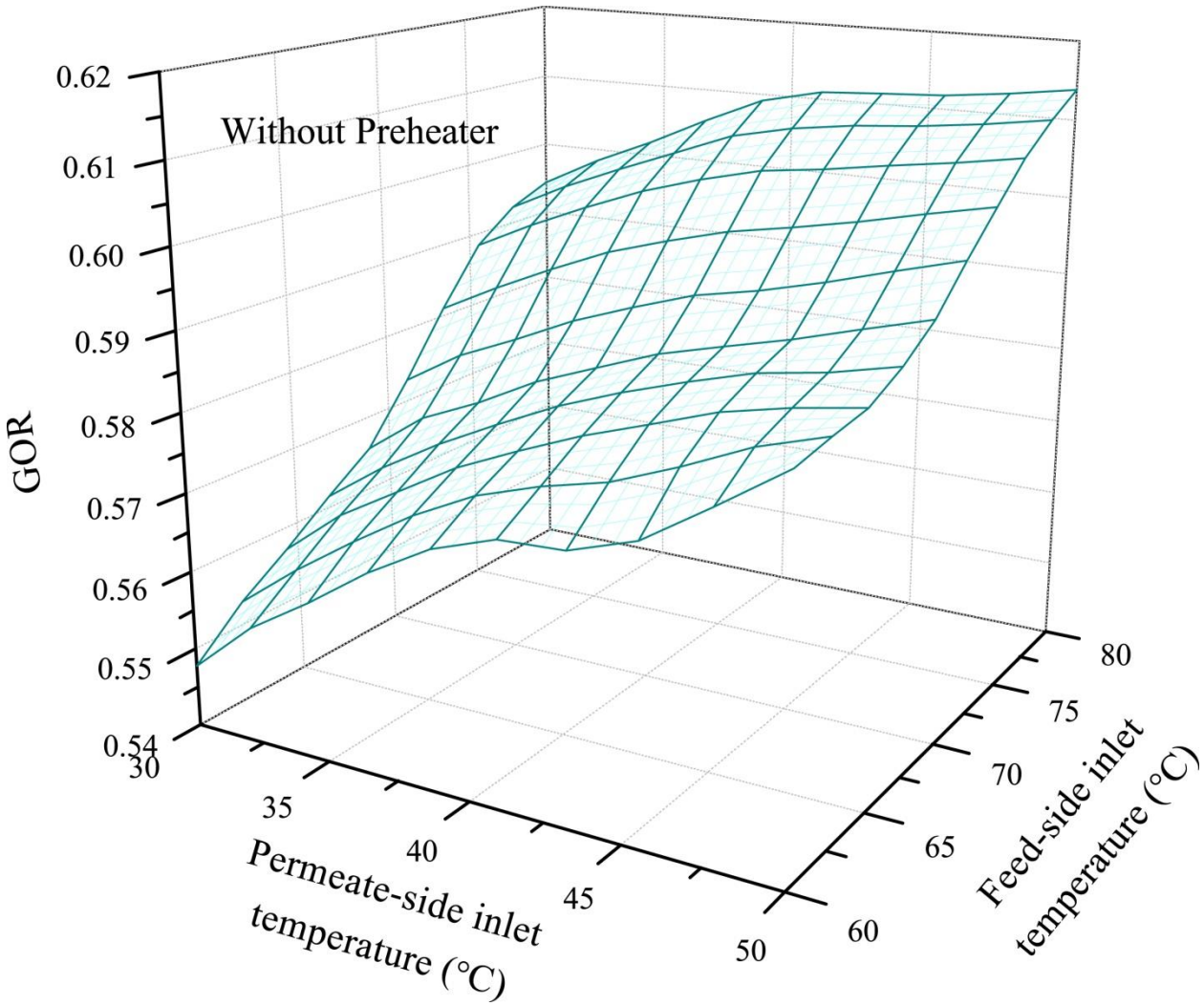

Figure 10: Energy efficiency (GOR) in MDC without heat recovery unit

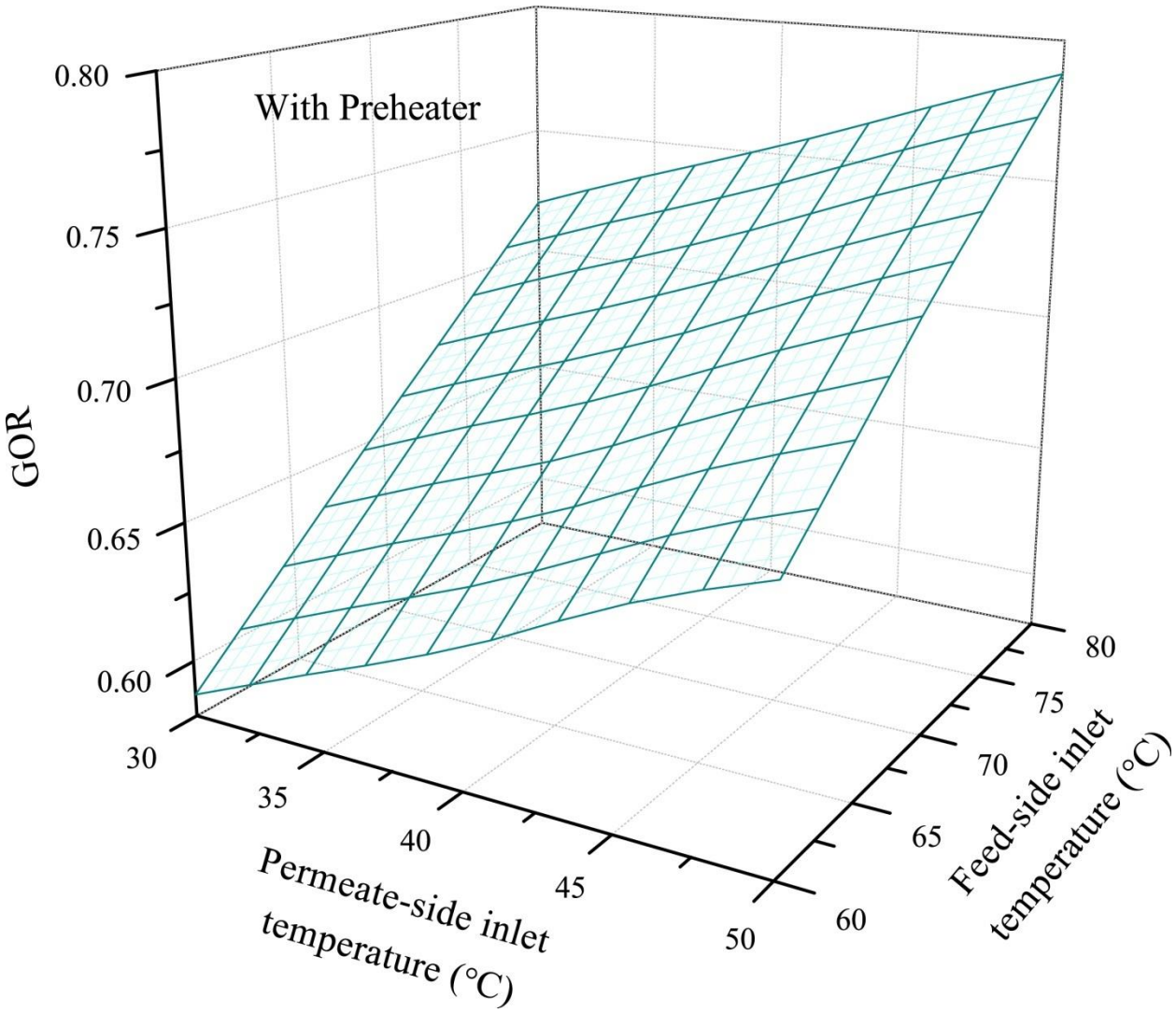

Figure 11: Energy efficiency (GOR) in MDC with heat recovery unit